Geology, published online on 3 July 2013 as doi:10.1130/G34505.1

Geology

Sinkhole precursors along the Dead Sea, Israel, revealed by SAR interferometry

Ran N. Nof, Gidon Baer, Alon Ziv, Eli Raz, Simone Atzori and Stefano Salvi

Geology published online 3 July 2013;
doi: 10.1130/G34505.1

Notes

Geology, published online on 3 July 2013 as doi:10.1130/G34505.1

Sinkhole precursors along the Dead Sea, Israel, revealed by SAR interferometry

Ran N. Nof[1,2,3], Gidon Baer[2], Alon Ziv[3], Eli Raz[4], Simone Atzori[5], and Stefano Salvi[5]
[1]Department of Geological and Environmental Sciences, Ben-Gurion University of the Negev, Mailbox 653, Beer-Sheva 84105, Israel
[2]Geological Survey of Israel, 30 Malkhe Israel Street, Jerusalem 95501, Israel
[3]Department of Geophysics and Planetary Sciences, Tel-Aviv University, Ramat-Aviv, Tel-Aviv 69978, Israel
[4]Dead Sea and Arava Science Center, Tamar Regional Council, Dead-Sea mobile post 86910, Israel
[5]Istituto Nazionale di Geofisica e Vulcanologia, Centro Nazionale Terremoti (CNT-INGV), Via di Vigna Murata 605, 00143 Rome, Italy

ABSTRACT

The water level in the Dead Sea (Israel and Jordan) has been dropping at an increasing rate since the 1960s, exceeding one meter per year during the last decade. This drop has triggered the formation of sinkholes and widespread land subsidence along the Dead Sea shoreline, resulting in severe economic loss and infrastructural damage. In this study, the spatiotemporal evolution of sinkhole-related subsidence and the effect of human activities and land perturbation on sinkhole development are examined through interferometric synthetic aperture radar measurements and field surveys conducted in Israel during 2012. Interferograms are generated using COSMO-SkyMed satellite images and a high-resolution (0.5 m/pixel) elevation model obtained from LiDAR measurements. As a result of this unique combination of high-resolution data sets, millimeter-scale subsidence has been resolved in both natural and human-disturbed environments. Precursory subsidence over a period of a few months occurred before the collapse of all three sinkhole sites reported in this study. The centers of the subsiding areas migrated, possibly due to progressive dissolution and widening of the underlying cavities. Filling of newly formed sinkholes with gravel, and mud injections into drill holes, seem to enhance land subsidence, enlarge existing sinkholes, and form new sinkholes. Apart from shedding light on the mechanical process, the results of this study may pave the way for the implementation of an operational sinkhole early-warning system.

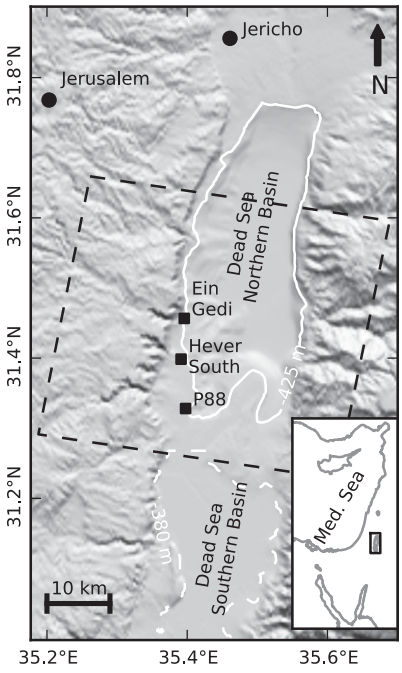

Figure 1. Location map of three sinkhole sites along the Dead Sea reported in this study. Black rectangles mark sites P88 (31.329°N, 35.397°E), Hever South (31.399°N, 35.391°E), and Ein-Gedi (31.457°N, 35.396°E). Black dashed line indicates area covered by the COSMO-SkyMed images. Dead Sea's northern and southern basins are marked by solid white contour at 425 m below mean sea level (msl) and dashed white contour at 380 m below msl, respectively. Hill-shaded digital elevation model is shown in background. Inset shows Dead Sea location in the eastern Mediterranean region.

INTRODUCTION

Sinkholes occur in diverse geological environments around the globe. Their most common formation mechanism is dissolution of soluble rocks and creation of subsurface cavities that collapse after becoming insufficiently supported (e.g., Waltham et al., 2005). The soluble rock may be carbonate (Sinclair, 1982), gypsum (Cooper and Waltham, 1999), or halite (e.g., Abelson et al., 2003). An additional cause for sinkhole formation is underground quarrying (e.g., Parise, 2012). Sinkholes have claimed lives in several catastrophic events (Bezuidenhout and Enslin, 1970) and caused severe economic losses (Gutiérrez et al., 2004).

The first identified sinkholes along the Dead Sea coast in Israel and Jordan (Fig. 1) appeared in the 1960s (Frumkin and Raz, 2001). Their occurrence rate has accelerated significantly, from less than 50 new sinkholes per year before 1999 to more than 380 per year since 2003 (Abelson and Gabay, 2009). Along the western coast of the Dead Sea, the sinkholes are clustered in ~50 sites, some comprising a few hundred sinkholes. The primary cause for sinkhole formation along the Dead Sea is the dissolution of an ~10,000-year-old salt layer that is 8–12 m thick and 20–50 m deep, and collapse of the strata overlying the newly formed cavities. The dissolution of this salt layer is due to the replacement of hypersaline groundwater by fresh groundwater in response to dropping of the Dead Sea water level (see Yechieli, 2000, for details). The rate at which the interface between the two groundwater masses is moving seaward is directly related to the rate of the sea-level drop, which is currently very high, ~1.3 m/yr.

Sinkholes pose a severe threat to the development of the Dead Sea region; a recreation site has been abandoned due to sinkhole formation, and injuries have been reported on several occasions (Frumkin and Raz, 2001). The increasing probability of sinkholes forming directly beneath heavily used facilities has led local and national authorities to carry out prevention and recovery actions, which have altered the natural processes and may have also affected sinkhole formation. These developments emphasize the need to improve our understanding of sinkhole formation mechanisms, and particularly to explore methods for detection of sinkhole precursors. In this study, we analyze the spatiotemporal evolution of sinkhole-related land subsidence using a combination of high-resolution interferometric synthetic aperture radar (InSAR) and LiDAR measurements. We identify distinct collapse-precursory subsidence, and present evidence for anthropogenic effects on sinkhole evolution.

INSAR-LIDAR DATA FUSION

Twenty-one (21) COSMO-SkyMed (CSK; http://www.e-geos.it/products/cosmo.html) X-band radar images (HIMAGE mode), acquired between 14 December 2011 and 1 January 2013, were processed to 20 geocoded interferograms (see Table DR1 in the GSA Data Repository[1])

[1]GSA Data Repository item 2013284, Table DR1 (list of available images, their relative perpendicular baselines, and altitude of ambiguity), Figure DR1 (signal enhancement using a hybrid DEM), Figure DR2 (consecutive interferograms of P88 sinkhole site), Figure DR3 (differential map between two LiDAR measurements at sinkhole site P88), Figure DR4 (consecutive interferograms of Hever South sinkhole site), and Figure DR5 (consecutive interferograms of Ein-Gedi sinkhole site), is available online at www.geosociety.org/pubs/ft2013.htm, or on request from editing@geosociety.org or Documents Secretary, GSA, P.O. Box 9140, Boulder, CO 80301, USA.

using the Gamma software (Wegmuller et al., 1998). The interferograms were generated at full resolution (pixel size of ~3 m) and filtered using an adaptive filter function that is based on the local fringe spectrum (Goldstein and Werner, 1998), with a window size of 16 × 16 pixels. Owing to the small size of the sinkholes (several meters), baseline re-estimation was not required, as this procedure corrects for distortions of longer wavelengths. The line-of-sight measurements (incidence angle of 41° from vertical, right-looking) were *a priori* interpreted as representing pure vertical movements, and were thus projected to vertical.

To geocode and remove the topographic phase components in the InSAR measurements, we first used the 1 arc-second ASTER (Advanced Spaceborne Thermal Emission and Reflection Radiometer) global digital elevation model (GDEM), which is considered to have a vertical accuracy of 17 m at 95% confidence level (Tachikawa et al., 2011). Because this

Figure 2. Photographs of the studied sinkholes. A: Aerial photo (view to the east) of sinkhole #88 at site P88, taken on 16 April 2012. White arrow indicates location of first collapse and gravel fill. Second collapse is visible to left of the first, at edge of gravel ramp (Photo: Assaf Tsabar). B: Sinkholes #134 (13 m long) and #143 at Hever South. Photo taken on 23 April 2013, view to the north. C: Renewed collapse (view to the east) at sinkhole #113 at Ein-Gedi, observed on 11 March 2013, shortly after it was filled by gravel.

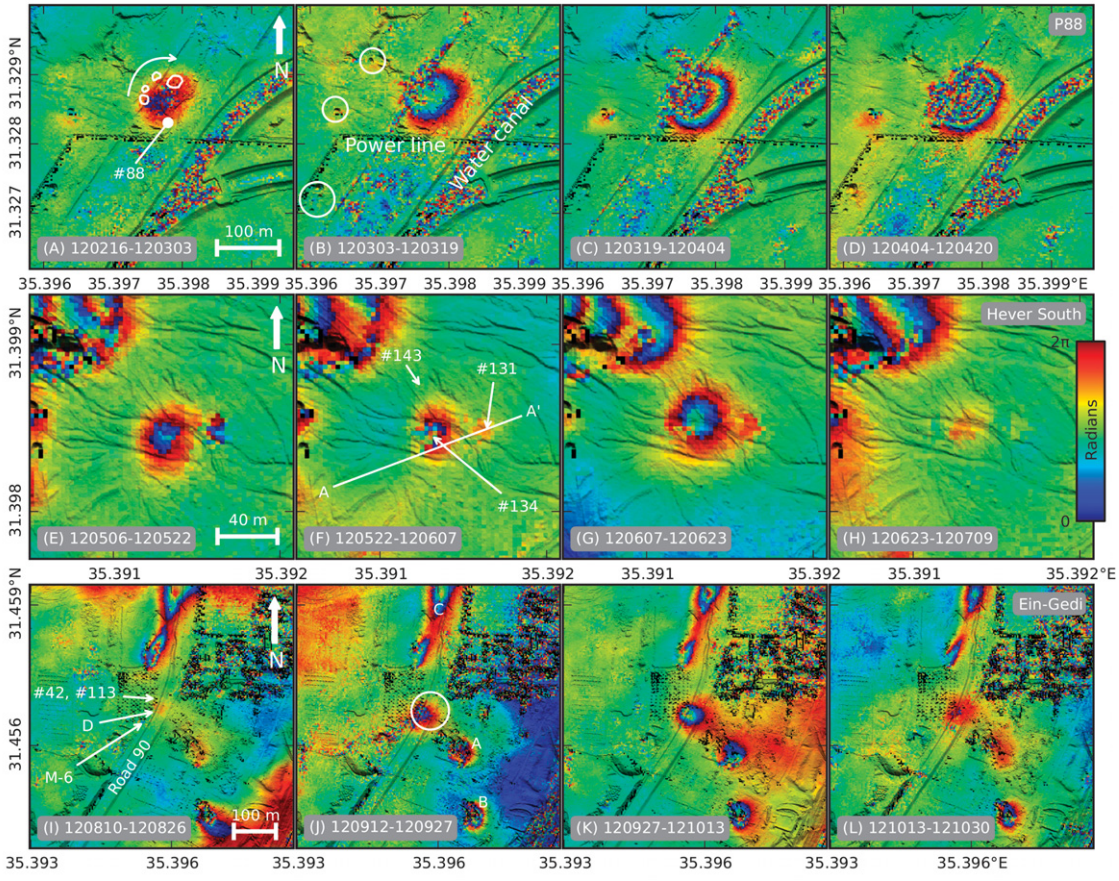

Figure 3. Interferograms of studied sinkhole sites, with one color cycle (blue-yellow-red) representing one-half of a radar wavelength (~1.5 cm) displacement away from satellite, along satellite line of sight. Top, middle, and bottom panels are for sites P88, Hever South, and Ein-Gedi, respectively. A: P88, 32–16 d before first sinkhole collapse. Sinkholes identified by differential LiDAR measurements are marked by white contours, and arrow indicates order in which they formed (see text and Fig. DR3 [see footnote 1]). Location used for cumulative displacement measurements shown in Figure 4A is indicated by #88. B: P88, 16 d prior, to a few hours after, first collapse. White circles mark nearby previous sinkholes. C: P88, a few hours to 16 d after first collapse. D: P88, 16–32 d after first collapse. E: Hever South, ~3 mo before collapse of sinkhole #134. F: Hever South, during sinkhole #134 collapse. White line A-A′ marks location of a cumulative displacement profile shown in Figure 4B, intersecting also a newly formed sinkhole #131. G: Hever South, shortly after collapse of sinkhole #134. Note that center of subsidence has migrated northward (see Fig. 2B). H: Hever South, between 2 and 4 weeks after sinkhole #134 collapse. Note that subsidence rate has decreased significantly. I: Ein-Gedi, 3–2.5 mo before widening of sinkhole #42. M-6 indicates borehole location. Location of cumulative displacement measurements shown in Figure 4A is labeled D. J: Ein-Gedi, period of mud injection. Circle marks subsiding area at Road 90. Ongoing subsidence areas are marked by A, B (abandoned recreation site), and C. K,L: Ein-Gedi, after drilling period. See text for more details.

DEM error is comparable to the altitude of ambiguity of many of the interferograms (Table DR1), use of the ASTER-only DEM gave rise to spurious structures (Figs. DR1A and DR1B in the Data Repository). In an attempt to minimize these errors, we used airborne LiDAR measurements taken in May 2011 to generate a digital surface model (DSM) with a spatial resolution of 0.5 m, an absolute elevation error of less than 0.35 m, and a spatial uncertainty of less than 1 m (Filin et al., 2011). One limitation of LiDAR DSMs is that elevation data include surface objects (e.g., power lines and vegetation), and their sharp relief may result in shadowed or overlaid areas where no interferometric phase can be calculated, resulting in data gaps. However, the composite ASTER-LiDAR DEM eliminates most of the topographic artifacts and dramatically increases the spatial resolution within the areas covered by LiDAR, thus enabling deformation monitoring at the spatial scale of individual sinkholes (Figs. DR1C and DR1D).

RESULTS

Here we present three examples of sinkhole-precursory subsidence and post-collapse ground displacements, and discuss the possible effects of human activities on sinkhole evolution.

Pumping Station P88

A new sinkhole (#88) formed on 19 March 2012, under a service road near the Dead Sea Works pumping station P88 (Figs. 1, 2A, and 3A–3D). Following the collapse event, the sinkhole was filled with 42 truckloads of gravel. Three subsequent collapse events occurred in adjacent locations during the following weeks, and all sinkholes were in turn filled with gravel. Interferograms spanning the period before, during, and after the formation of the sinkholes reveal subsidence around the sinkholes during the entire interval from December 2011 to January 2013 (Figs. 3A–3D; Fig. DR2). Subsidence began at least 3 mo before the first sinkhole collapse and continued for at least 9 mo thereafter. Interferograms that include or post-date the time of the sinkhole formation show increasing coherence loss due to extensive road works (Fig. DR2). The spatial extent of the subsiding area has not changed significantly with time. Interestingly, the first sinkhole formed near the western margin of the subsiding zone, rather than at its center. A differential map between two LiDAR measurements taken in May 2012 and May 2011 (Fig. DR3) reveals spatial migration of successive sinkholes, possibly indicating progressive dissolution at the underlying cavity.

A time series of cumulative subsidence in an area that is unaffected by road works (Fig. 4A) indicates a significant increase in subsidence rate from less than 0.5 mm/day before the first collapse to more than 4 mm/day ~3 mo after the collapse events, and deceleration thereafter. The question as to whether the subsidence rate has been enhanced by the gravel fill is yet unresolved.

Hever South

The Hever South sinkhole site (Fig. 1) is among the most active sites in the Dead Sea area. Routine field surveys are being carried out every 3 mo to identify new sinkholes and monitor their development. Ongoing subsidence and sinkhole formation were observed in the entire Hever South site during 2012 (Fig. DR4). An elliptic, 13-m-long and 7-m-deep sinkhole (#134, Fig. 2B) was formed between 22 May and 7 June 2012 (see coherence loss at the center of the subsiding area in Fig. 3F). In this specific location, subsidence had already begun a few months before the sinkhole collapsed. The size of the subsiding area increased until the collapse of the sinkhole, and remained almost constant thereafter (Fig. 4B). The center of the subsiding area migrated northward (compare Figs. 3E and 3G; see Fig. DR4), suggesting northward expansion of the subsurface cavity. An additional sinkhole (#143) appeared at the northern end of this subsiding area in mid-February 2013 (Figs. 2B and 3F). The subsidence rate started accelerating ~6 weeks before the collapse of the sinkhole (Fig. 4A). In contrast with sinkhole #88, where the subsidence rate increased after sinkhole formation, the subsidence rate in Hever South sinkhole #134 decelerated after the collapse of the first sinkhole (Fig. 3H).

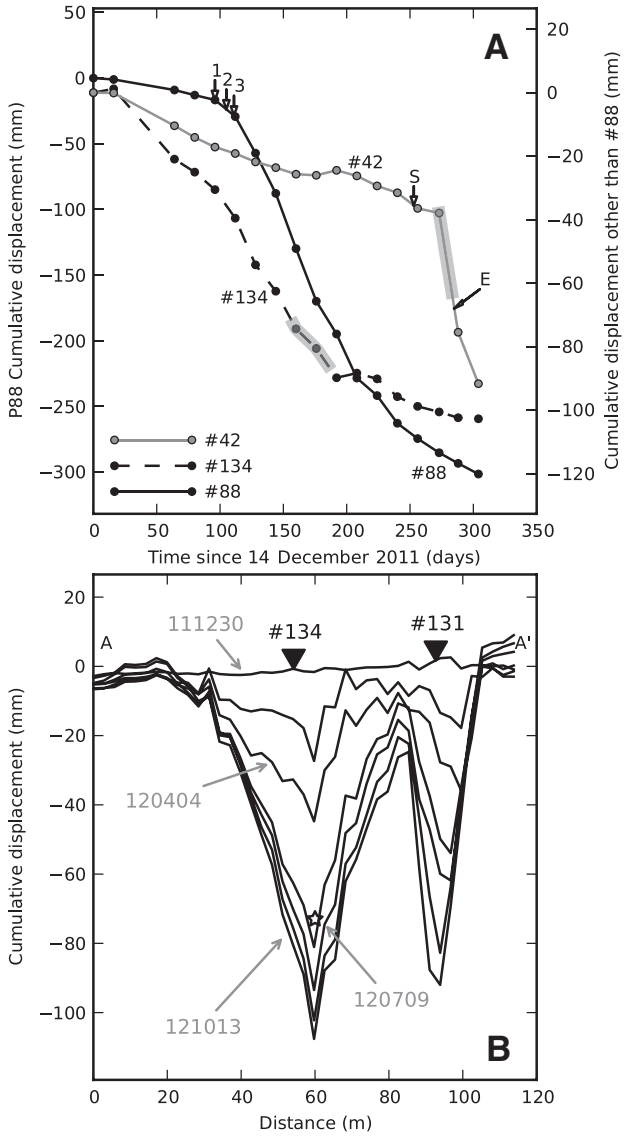

Figure 4. A: Cumulative displacements at sinkhole sites, with left-side axis for the P88 site and right-side axis for other sites. Vertical arrows labeled 1, 2, and 3 mark recorded collapse dates at sinkhole #88. Estimated collapse interval of sinkhole #134 is highlighted in gray. S and E mark start and end times, respectively, of drilling in borehole M-6 in Ein-Gedi. Interval during which mud was injected into borehole is highlighted in gray on Ein-Gedi displacement curve. B: Profiles of cumulative displacement along a traverse crossing sinkholes #134 and #131 at Hever South (see profile location in Fig. 3F). Lines represent cumulative displacement between 14 December 2011 and 13 October 2012, at 48 d intervals. Dates in YYMMDD. Star marks time and location of sinkhole #134 collapse.

The Ein-Gedi Sinkhole Lineament

The Ein-Gedi sinkhole lineament strikes subparallel to the main Dead Sea Road (Figs. 1 and 3I–3L). It has been active since the mid 1990s, causing extensive destruction to the (now-abandoned) Ein-Gedi recreation village and the nearby palm plantations. In 2002, the road infrastructure was reinforced and covered by geosynthetics, in an attempt to prevent or delay the formation of sinkholes at the intersection between the sinkhole lineament and the main road. Since then, while

sinkholes continued forming along the entire lineament, none were formed at the intersection. The Ein-Gedi sinkhole lineament is undergoing gradual subsidence at rates of 0.5–2 mm/day, as observed in the CSK interferograms since the end of 2011 (Fig. DR5). Prior to 12 September 2012, only minor subsidence of ~0.1 mm/day occurred at the lineament-road intersection (Fig. 3I; Fig. DR5). From 12 September to 13 October 2012, the subsidence rate along the road increased to ~2 mm/day, and decreased thereafter. An existing sinkhole (#42) has been active since 2002, ~15 m west of the road at the margin of this subsidence area (Fig. 3I), and its width increased notably between 14 September and 15 October 2012. Approximately 3 mo after the dramatic increase in subsidence rate, a new sinkhole (#113) formed ~7 m NNE of sinkhole #42 (Figs. 2C and 3I). Despite the repeated filling of these sinkholes with gravel since December 2012, their growth continues.

An observational borehole was drilled by the Israeli National Roads Company between 23 August and 24 September 2012, ~50 m south of sinkhole #42 (Fig. 3I). Injection of mud and loss of drill circulation occurred several times between 12 and 23 September (Fig. 4A) at depths of between 39 and 63 m (L. Kirshner, 2012, personal commun.), probably due to leakage into adjacent cavities. The period of increased subsidence rate (Figs. 3J and 4A) coincides with the time of circulation loss at the borehole, and with the dramatic increase in the size of the sinkhole. This coincidence strongly suggests that, in contrast with the P88 and Hever South sinkholes that formed within relatively undisturbed environments, land subsidence and sinkhole expansion within the Ein-Gedi site are locally affected by human activity. While it seems that the intensive geotechnical reinforcement of the road during the years 2002–2012 successfully reduced subsidence and sinkhole collapses, the drilling seems to have triggered sinkhole activity.

DISCUSSION AND CONCLUSIONS

Previous studies showed a spatial association between gradual subsidence and sinkholes (Baer et al., 2002; Abelson et al., 2003), yet the temporal relationship between the two features was undetermined due to poor spatiotemporal resolution of the available InSAR measurements. CSK interferograms generated with the LiDAR-based DEM reduced the topographic artifacts and dramatically improved the spatial and temporal resolving power of these InSAR measurements (Fig. DR1), enabling the use of short-temporal interferograms even with long perpendicular baselines. Our study reveals millimeter-scale localized subsidence over a few months preceding sinkhole formation. The sinkholes formed either at the margins of the subsiding areas or close to their centers. In addition, the subsidence areas and/or the sinkholes migrated, possibly as a result of progressive dissolution and widening of subsurface cavities. In the undisturbed natural environment of Hever South sinkhole #134, the subsidence rate accelerated before sinkhole collapse, and decelerated thereafter. In sinkhole #88, human intervention after the sinkhole collapse was followed by an increase in the subsidence rate. In the disturbed environment of the Ein-Gedi sinkhole lineament, accelerated subsidence preceded the collapse of the sinkholes, and both were most likely triggered by drilling and mud injection at a nearby borehole.

While the present study is based on a limited data set, our results clearly indicate that mapping of ground displacement may serve to identify the location of future sinkholes, and can be incorporated into a sinkhole early-warning algorithm. A semi-automatic algorithm is currently under test, and its performance in terms of false, missed, or true alarm will be determined as additional data become available.

ACKNOWLEDGMENTS

We thank Ellen Thomas, Shimon Wdowinski, and three anonymous reviewers for their thorough reviews, which significantly improved this paper. The project was carried out using CSK® products, ©ASI (the Italian Space Agency), delivered under an ASI license. The ASTER GDEM is a product of The Ministry of Economy, Trade and Industry of Japan (METI) and NASA. Lidar 2011 measurements were carried out by SEE Advanced Mapping Systems and Solutions Ltd. (Israel), and the 2012 Lidar data were kindly shared with us by the Dead Sea Drainage Authority. We thank L. Kirshner from the Israeli National Roads Company for the Ein-Gedi drilling reports.

REFERENCES CITED

Abelson, M., and Gabay, R., 2009, Evolution of the Dead Sea sinkholes between August 2006 and December 2008—Scan of aerial photographs: Geological Survey of Israel Report TR-GSI/13/2009, 15 p.

Abelson, M., Baer, G., Shtivelman, V., Wachs, D., Raz, E., Crouvi, O., Kurzon, I., and Yechieli, Y., 2003, Collapse-sinkholes and radar interferometry reveal neotectonics concealed within the Dead Sea basin: Geophysical Research Letters, v. 30, 1545, doi:10.1029/2003GL017103.

Baer, G., Schattner, U., Wachs, D., Sandwell, D., Wdowinski, S., and Frydman, S., 2002, The lowest place on Earth is subsiding—An InSAR (interferometric synthetic aperture radar) perspective: Geological Society of America Bulletin, v. 114, p. 12–23, doi:10.1130/0016-7606(2002)114<0012:TLPOEI>2.0.CO;2.

Bezuidenhout, C.A., and Enslin, J.F., 1970, Surface subsidence and sinkholes in the dolomitic area of the Far West Rand, Transvaal, Republic of South Africa, *in* Proceedings of the International Symposium on Land Subsidence, Tokyo, September 1969: International Association of Hydrological Sciences Publication 89, p. 482–495.

Cooper, A.H., and Waltham, A.C., 1999, Subsidence caused by gypsum dissolution at Ripon, North Yorkshire: Quarterly Journal of Engineering Geology and Hydrogeology, v. 32, p. 305–310, doi:10.1144/GSL.QJEG.1999.032.P4.01.

Filin, S., Baruch, A., Avni, Y., and Marco, S., 2011, Sinkhole characterization in the Dead Sea area using airborne laser scanning: Natural Hazards, v. 58, p. 1135–1154, doi:10.1007/s11069-011-9718-7.

Frumkin, A., and Raz, E., 2001, Collapse and subsidence associated with salt karstification along the Dead Sea: Carbonates and Evaporites, v. 16, p. 117–130, doi:10.1007/BF03175830.

Goldstein, R.M., and Werner, C.L., 1998, Radar interferogram filtering for geophysical applications: Geophysical Research Letters, v. 25, p. 4035–4038, doi:10.1029/1998GL900033.

Gutiérrez, F., Lucha, P., and Guerrero, J., 2004, La dolina de colapso de la casa azul de Calatayud (noviembre de 2003): Origen, efectos y pronóstico, *in* Benito, G., and Díez-Herrero, A., eds., Riesgos naturales y antrópicos en Geomorfología, VII: Toledo, Spain, Reunión Nacional de Geomorfología, p. 477–488.

Parise, M., 2012, A present risk from past activities: Sinkhole occurrence above underground quarries: Carbonates and Evaporites, v. 27, p. 109–118, doi: 10.1007/s13146-012-0088-3.

Sinclair, W.C., 1982, Sinkhole development resulting from ground-water withdrawal in the Tampa area, Florida: U.S. Geological Survey Water-Resources Investigations 81-50, 19 p.

Tachikawa, T., Hato, M., Kaku, M., and Iwasaki, A., 2011, Characteristics of ASTER GDEM version 2, *in* Proceedings of the 2011 IEEE Geoscience and Remote Sensing Symposium, 24–29 July 2011, Vancouver, Canada: Piscataway, New Jersey, Institute of Electrical and Electronics Engineers, p. 3657–3660, doi:10.1109/IGARSS.2011.6050017.

Waltham, T., Bell, F.G., and Culshaw, M.G., 2005, Sinkholes and Subsidence: Karst and Cavernous Rocks in Engineering and Construction: Chichester, UK, Springer, 382 p.

Wegmuller, U., Werner, C., and Strozzi, T., 1998, SAR interferometric and differential interferometric processing chain, *in* Proceedings, 1998 IEEE Geoscience and Remote Sensing Symposium, 6–10 July 1998, Seattle, Washington, Volume 2: Piscataway, New Jersey, Institute of Electrical and Electronics Engineers, p. 1106–1108.

Yechieli, Y., 2000, Fresh-saline ground water interface in the western Dead Sea area: Ground Water, v. 38, p. 615–623, doi:10.1111/j.1745-6584.2000.tb00253.x.

Manuscript received 20 February 2013
Revised manuscript received 15 May 2013
Manuscript accepted 17 May 2013

Printed in USA